In-situ STM and XRD studies on Nb–H films: Coherent and incoherent phase transitions

ARTICLE *in* JOURNAL OF ALLOYS AND COMPOUNDS · DECEMBER 2014

Impact Factor: 3 · DOI: 10.1016/j.jallcom.2014.12.103

3 AUTHORS, INCLUDING:

Vladimir Burlaka

Georg-August-Universität Göttingen

7 PUBLICATIONS **17** CITATIONS

SEE PROFILE

A. Pundt

Georg-August-Universität Göttingen

117 PUBLICATIONS **1,666** CITATIONS

SEE PROFILE

Journal of Alloys and Compounds 645 (2015) S388–S391

Contents lists available at ScienceDirect

Journal of Alloys and Compounds

journal homepage: www.elsevier.com/locate/jalcom

In-situ STM and XRD studies on Nb–H films: Coherent and incoherent phase transitions

Vladimir Burlaka *, Stefan Wagner, Astrid Pundt

Institut für Materialphysik, Universität Göttingen, Friedrich-Hund-Platz 1, D-37077 Göttingen, Germany

ARTICLE INFO

Article history:
Available online 23 December 2014

Keywords:
Thin films
Precipitation
Phase transition
Interstitial alloys
Scanning Tunnelling Microscopy (STM)
X-ray diffraction (XRD)

ABSTRACT

Hydride precipitation in 25 nm and 40 nm epitaxial Nb-films was studied by Scanning Tunnelling Microscopy (STM) supported by X-ray diffraction (XRD) measurements. In combination, these methods yield information about the phase transition, the coherency state, the hydride precipitates' density and size as well as their lateral distribution, at 293 K. For both film thicknesses, hydride formation was detected with STM; it can be easily missed by XRD. While the 25 nm film showed a coherent phase transition, the phase transition was incoherent for the 40 nm film. This is in good accordance with theory. The phase transition features are found to strongly depend on the coherency state: a large number of small hydrides appear in the coherent regime while a small number of large hydrides evolve in the incoherent regime.

1. Introduction

Phase transformations of metal–hydrogen (M–H) films differ from those of the bulk M–H systems. M–H films often show a strong adhesion to the substrate causing anisotropic lattice expansion and in-plane mechanical stresses in the GPa range [1–5]. In thin films, the lattice expansion mainly occurs in the out-of-plane direction and, therefore, leads to a film surface corrugation. When the film contains locally different hydrogen concentrations, such as could be caused by the presence of different phases, the position of these phases can be determined by monitoring the differences in local lattice expansion, i.e. by measuring the related nano-scale surface corrugations by in-situ STM [6–9]. Simultaneously, the phase transformation processes, especially hydride phase precipitation and the related lattice parameter changes caused by hydrogen absorption, can be studied on the macro scale, i.e. by measuring XRD patterns.

Stresses which arise during hydrogen absorption in the film can be partly released via plastic deformation. This causes irreversible lattice deteriorations [4–6,10–12] and surface roughening [8,9]. Dislocation formation can occur at the hydride/α-matrix interface [4,5,9,10,13] as well as at the hydride/substrate interface [10, 14–16]. Nörthemann et al. [9] recently posited the existence of a critical film thickness, d_c, below which the stress release efficiency would change drastically. For systems with thickness greater than d_c, mechanical stress can be released by the incorporation of misfit dislocations, resulting in formation of irreversible incoherent phase boundaries. For systems below d_c, mechanical stress arising between the different phases cannot be released, since dislocation occurrence is not energetically favourable [4,5,17]. These systems stay coherent throughout the complete phase transition [9,11,18–20]. The first evidence for the absence of dislocation loops around hydrides in thin films were recently found for Pd–H films of about 22 nm film thickness [11].

For Nb–H thin films, Nörthemann et al. calculated the critical size separating the coherent and the semi-coherent phase transformation by comparing the accumulated strain energies of a coherent cylindrical hydride precipitate in a Nb-film to the self-energy of a dislocation loop E_{loop} of radius r located around it [9,17]. For the determination of $E_{loop}(r)$, Kroupa's approach was applied [21]. Based on these calculations, Nörthemann et al. suggested that for Nb films of $d < d_c = 26$ nm, the formation of dislocations at the hydride-matrix interface is energetically not favourable [9]. However, this prediction of Nörthemann et al. has not been proven experimentally. Thus, in this work, Nb–H films of 25 nm and 40 nm thickness are used to prove the presence of a critical thickness, as well as to examine the effect of stress release on hydride precipitation and growth [19,22]. In summary, the system is used to elucidate the effect of the coherency state on hydride precipitation and growth.

2. Experimental details

(110) oriented epitaxial Nb films of 25 nm and 40 nm thicknesses were prepared by Ar ion-beam sputtering on polished Al_2O_3 substrates with (11–20) surface orientation, provided by CrysTec GmbH. The substrates had a miscut of less

* Corresponding author. Tel.: +49 0551 39 5024.
E-mail address: vburlaka@material.physik.uni-goettingen.de (V. Burlaka).

http://dx.doi.org/10.1016/j.jallcom.2014.12.103
0925-8388/

than 0.1°. Film preparation was performed in an UHV sputter system containing a background pressure better than 1.5×10^{-10} mbar. Sputtering was performed at 2×10^{-4} mbar Ar pressure (Ar purity 99.9999%). High purity niobium (99.99%) was used as target material (deposition rate 0.7 ± 0.1 nm/min). The films were prepared at 760–800 °C. After Nb sputtering, the films were cooled down for 1.5–2 h to reach a substrate temperature of less than 35 °C. To facilitate hydrogen absorption at RT, a Pd catalyst of less than 0.5 monolayer thickness was deposited onto the Nb films after cooling down to 35 °C [8].

In-situ Scanning Tunnelling Microscopy (STM) measurements and continuous gas loading experiments were performed using a UHV-MICRO-STM system by OMICRON under UHV conditions immediately after film preparation, without exposing the samples to air. The STM-measurements were done in constant current mode by the use of mechanically thinned Pt/Ir tips. During the long-time STM measurements, the hydrogen gas pressure p_H was kept constant for a certain loading time t. When no topographical changes were detected after about 5 h, the hydrogen pressure was increased to a new constant value. Exposure times t at the new pressure are given relative to the moment of pressure increase.

For films undergoing studies outside of the deposition/STM system, such as for in-situ hydrogen gas loading XRD, the surface was covered with a 20 nm Pd capping layer (Pd-target of 99.95% purity). The Pd deposition rate was (2.1 ± 0.1) nm/min. This thick capping layer was required to prevent subsequent film oxidation.

The in-situ hydrogen gas loading XRD measurements were performed at the Synchrotron facility in Grenoble (ESRF) at beam line BM20 (λ = 1.0781 Å) and in Hamburg (Desy/Petra III) at beam line PO8 (λ = 0.98188 Å, λ = 0.99987 Å). A portative vacuum chamber was used to perform the constant flow hydrogen loading experiments. The shift of the Nb (1 1 0) XRD pattern in Bragg geometry was measured as a function of the film thickness, the hydrogen pressure and the exposure time.

3. Results and discussion

Fig. 1 shows STM images of the surface topography of the 40 nm Nb film before (Fig. 1(a) and during hydrogen loading (Fig. 1(b) and (c)). Fig. 1(b) ($p_H = 8 \times 10^{-7}$, t = 240 min) and Fig. 1(c) ($p_H = 1.6 \times 10^{-6}$, t = 100 min) show the surface topography during hydrogen loading at different hydrogen pressures p_H and exposure times t at given p_H. While the surface topography of the film is flat in Fig. 1(a) with a typical roughness of 0.18 nm (rms), elevated (bright) regions are detected in Fig. 1(b) and (c). The elevation is about 3 nm from the base film surface level. These regions correspond to locally formed hydride precipitates in the film and result from the related vertical volume expansion [9]. As such surface topographies result from underlying hydride precipitates in the film [9], we include at this point in the description the development of the hydrides precipitates themselves. For the 40 nm film, the hydride precipitates in the film expand and reach lateral sizes of about 500 nm, as shown in Fig. 1(c). For the initial growth stage, the lateral extension of the hydrides is of circular shape. For the later growth stages, the lateral extension of the hydrides becomes more irregular. Both types of growth stages can be seen in Fig. 1(c). This result is in accordance with those of the Nörthemann et al. studies of thicker Nb films [17]. Nörthemann suggested that the irregular morphology originates from preferred hydride growth in mechanically soft lattice directions [17]. Irregular hydride morphologies may also originate from the direction-dependency of plastic deformation [23]. The average distance between the neighbouring hydride precipitates ranges from 500 nm to 750 nm (Fig. 1(c)).

The STM surface topography of the 25 nm Nb film is shown in Fig. 2. Fig. 2(a) presents the topography before loading and Fig. 2(b) after loading at $p_H = 8 \times 10^{-7}$ mbar for t = 500 min. Elevated (bright) regions, as before, correspond to local hydride precipitates in the film and the related volume expansion. According to these images, hydride formation clearly appears in the 25 nm film.

Because the amplitude of the surface corrugation becomes smaller with decreasing film thickness (2–3 nm for the 40 nm film and just 1–1.5 nm for the 25 nm film), the topography change becomes difficult to see in the original images. Therefore, Fig. 2(c) is a difference image comparing two intermediate states which highlights the absolute surface corrugation change (Fig. 2(c)). According to this difference image, the hydride precipitates reach a lateral size of about 50 nm, for the 25 nm film. Hydride precipitates seem to stay "locked-in size". For thicker films, a similar finding of hydrides being "locked-in size" was attributed to the vertical coherent lattice matching between the hydride precipitates and the remaining α-phase [17]. The "locked-in size" is linked to the largest coherent hydride detected. According to Nörthemann et al. and Kumar et al., the formation of larger precipitates requires dislocation formation [17,24]. Thus, we attribute our finding to the coherency state remaining in the 25 nm film and inhibiting the formation of the requisite dislocations for continued hydride growth. The surface corrugations are approximately circular in shape. The average distance between the neighbouring hydrides ranges from 50 nm to 100 nm (see Fig. 2(c)).

Further analyses of the surface corrugation of the 25 nm Nb thin film hint at additional plastic deformation processes, resulting from mechanical stress arising between the film and the substrate [11]. This stress relaxation mechanism requires more in-depth consideration. It will be discussed in the frame of another paper.

The differing appearances of the hydrides forming for the 25 nm film and for the 40 nm film are compared in Fig. 3. The pressure for both experiments was about $p_H = 1.6 \times 10^{-6}$ mbar. For the 25 nm film, shown in Fig. 3(a), a large number of small precipitates were found. The lateral size of the hydrides was about 50 nm, the "locked-in size", and approximately circular in shape. Upon hydrogen loading, the number density of hydrides increased. In contrast to this, the 40 nm film in Fig. 3(b) shows a small number of large hydrides. Upon hydrogen loading, these hydrides continued to grow. The related surface corrugation suggests that the hydrides are irregular in shape. The height difference in the topography of the two samples is illustrated in the height histograms, added in an inset for each picture (see Fig. 3(a) and (b)). For the 40 nm film, two independent peaks corresponding to Nb α-phase (high

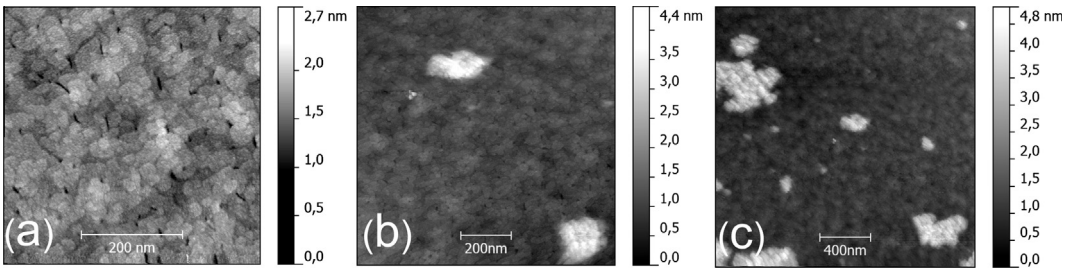

Fig. 1. STM surface-image of a 40 nm Nb film (a) before hydrogen loading ($p_H < 1 \times 10^{-9}$ mbar), and during hydrogen loading (b) at $p_H = 8 \times 10^{-7}$ mbar for t = 240 min, and (c) at $p_H = 1.6 \times 10^{-6}$ mbar for a further t = 100 min (total hydrogen exposure time of 340 min). Only a small number of hydride precipitates is visible. They grow to large lateral sizes of about 500 nm. The average distance between neighbouring hydrides is about 500–750 nm. (Frame sizes change from (a) 500 nm × 500 nm, to (b) 1000 nm × 1000 nm and (c) 2000 nm × 2000 nm. Also note the change in colour scale between images.)

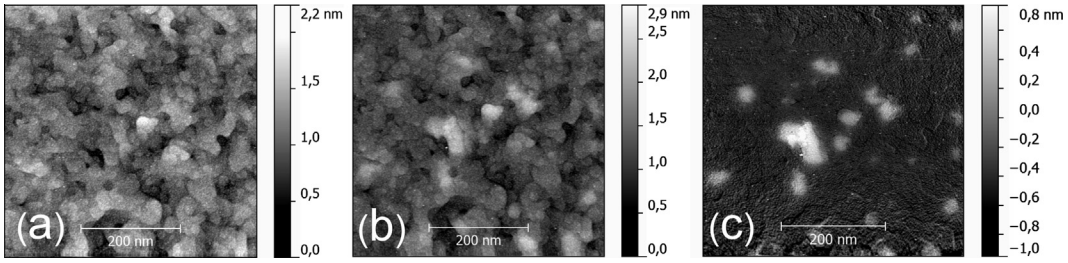

Fig. 2. STM surface-image of a 25 nm Nb film (a) before hydrogen loading ($p_H < 1 \times 10^{-9}$ mbar) and (b) during hydrogen loading at $p_H = 8 \times 10^{-7}$ mbar for $t = 500$ min. (c) Difference image: the hydride precipitates have a lateral size of about 50 nm; the average distance between neighbouring hydrides is about 50–100 nm. (Frame size: 500 nm × 500 nm. Note the change in the colour scale between images.)

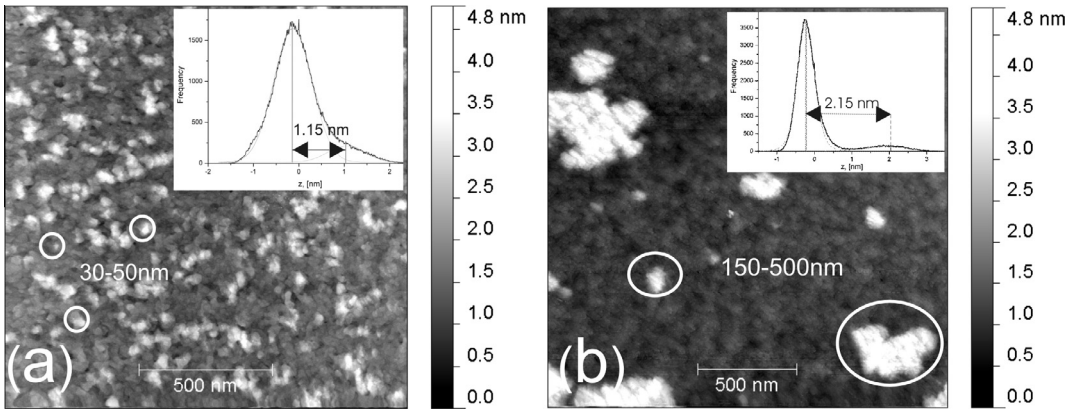

Fig. 3. (a) STM surface-image of 25 nm Nb after extended hydrogen loading at $p_H = 1.6 \times 10^{-6}$ mbar. A large number density of small hydrides (30–50 nm in lateral size) is found. Inset: The height histogram shows two close peaks, separated by 1.15 nm. (b) STM surface-image of 40 nm Nb after extended hydrogen loading at $p_H = 1.6 \times 10^{-6}$ mbar. A small number of large hydrides with sizes of up to 500 nm in lateral size is visible. Inset: The height histogram shows two peaks separated by 2.15 nm. (Frame size: (a) 1500 nm × 1500 nm and (b) 2000 nm × 2000 nm.)

intensity) and to the hydride-phase (low intensity) are clearly visible. These two peaks are separated by about 2.2 nm. For the 25 nm film, the peak separation is not pronounced and only a small shoulder related to the hydride phase is slightly visible. After the curve fitting (Gauss), the peak splitting in the height histogram was found to be only 1.15 nm. Also, the related surface corrugation is smaller for the thinner film. As the height difference roughly scales with the film thickness we cannot draw conclusions about the hydride coherency from the local film expansion in these images. However, the finding of the 'locked-in size' suggests the formation of coherent hydrides for the 25 nm film.

In-situ XRD measurements show a strong difference in the X-ray patterns of the two films. This can be seen in Fig. 4, which shows the peak development for different stages of hydrogen loading. For the 40 nm film, presented in Fig. 4(a), the α-phase and the hydride phase (β) related peaks are well separated. Upon hydrogen loading, the α-phase peak initially moves to the left because of lattice expansion. By further increasing the hydrogen concentration, the hydride peak appears and the intensity of the α-phase peak lowers. On continued loading, the intensity of the hydride-phase peak increases. The positions of the α-phase peak and the hydride phase peak are constant in the two phase region. This shows that the two phases behave independently, as is expected for incoherent phases.

For the 25 nm film, only one peak is observed, as shown in Fig. 4(b). This one broad peak moves towards lower 2θ angles upon hydrogen loading (Fig. 4(b)). No additional hydride peak appears in the pattern. Thus, in the XRD pattern of the 25 nm Nb–H film, the phase separation, as seen in the STM measurements, can be easily missed [25–28]. Only peak broadening and maximum intensity change hint on the presence of the hydride. Similar behaviour was reported in literature before, for coherent decomposed systems [29–31]. Gente et al. [29] and Busch et al. [30] observed in their studies on Cu–Co alloys only one XRD peak while the sample consisted of phase-separated (fcc) Cu- and (fcc) Co-rich regions. The separated regions were found to be coherently linked and small in size [29,30]. A single broad lattice reflection was also reported for coherent Cu–Co multi-layers, below a layer thickness of 8 nm [31]. According to Michaelsen, the different layers become XRD-invisible because of the lattice coherency.

Based on these results, the XRD-invisibility of the secondary phases in the 25 nm Nb–H film may be attributed to the coherent lattice matching between the α-phase and the hydride phase in combination with a high number density of small precipitates, distributed homogeneously in the α-matrix. Thereby, the α-phase is strained by the presence of the hydride precipitates and the hydrides are compressed by the surrounding α-matrix. This leads to peak broadening upon hydrogen loading and, to a continuous peak shift which depends on the volume fraction of hydrides. If the phases were matched incoherently, the peak profile would change asymmetrically upon hydrogen loading in the two phase region. This is not observed in Fig. 4(b). Thus, coherency and the small precipitate size make it difficult to separate the two phases and may be misinterpreted as the absence of phase separation.

Above the critical thickness, incoherency and larger hydride sizes make the two phases well separated in the XRD pattern such that phase separation can be easily detected.

In summary, the different peak development observed for the different thicknesses suggests coherent precipitation in the 25 nm film and incoherent precipitation in the 40 nm film.

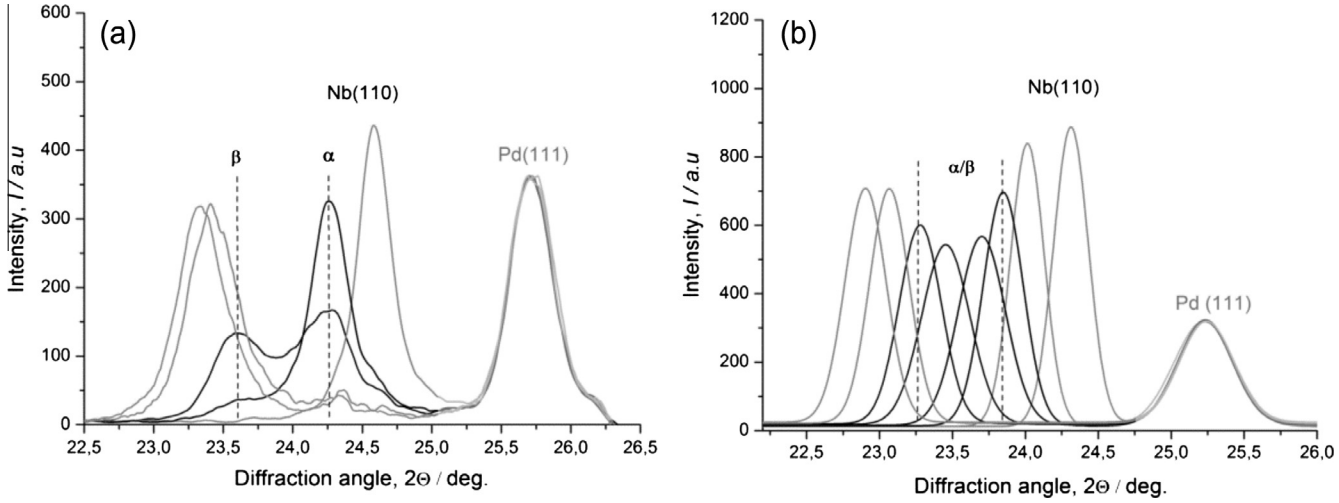

Fig. 4. XRD pattern upon hydrogen loading of Nb–H films, of (a) 40 nm and (b) 25 nm film thickness. The XRD patterns related to the single phase regions are plotted in light grey, while the patterns of the two-phase region are plotted in dark grey curves. For both films, the Nb (1 1 0) peak shifts to lower angles because of the lattice expansion upon hydrogen absorption. The Pd (1 1 1) peak position is constant. Differences appear in the two-phase regions: (a) Two well-separated peaks corresponding to the α- and the β-phase are visible in the two-phase region. Their peak positions are marked with dashed lines (λ = 0.99987 Å). (b) Only one broadened peak is detected in the two-phase region. It shifts to lower angles and its maximum intensity changes (λ = 0.98188 Å). The peak positions related to the borders of the two-phase region are marked with dashed lines. The phase-separation becomes nearly XRD-invisible.

4. Conclusions

The STM and XRD study on Nb–H thin films confirms the presence of a phase transition in the 40 nm and the 25 nm films. These results confirm the existence of the critical film thickness d_c suggested by Nörthemann et al. [9], separating the coherent phase transition regime from the incoherent regime. For Nb–H thin films, the critical thickness is between 25 nm and 40 nm, which is in good agreement with the calculated value of d_c = 26 nm. The STM measurements have shown that the coherency contribution strongly affects the hydride precipitation and growth mode. Below the critical thickness, in the coherent regime, the phase transformation is governed by nucleation, while above the critical thickness, the transformation is growth-controlled. We expect a critical thickness separating two different precipitation and growth regimes to occur in many other M–H thin film systems. However, the exact value of the related critical thickness is determined by the lattice mismatch between the solid solution and the hydride phase of the system, their elastic properties and the dislocation formation energy.

Acknowledgements

This research is kindly supported by the Deutsche Forschungsgemeinschaft (DFG, German Research Foundation) via the projects PU131/9-1 and PU131/12-1. Beamtime was kindly provided by ESRF at BM20 and DESY at P08. The helpful support of C. Bähtz and O. Seeck is gratefully acknowledged. M. L. Martin at University of Göttingen is gratefully acknowledged for discussions on this paper.

References

[1] P.F. Miceli, H. Zabel, J.A. Dura, C.P. Flynn, J. Mater. Res. 6 (1991) 964.
[2] Q.M. Yang, G. Schmitz, S. Fähler, H.U. Krebs, R. Kirchheim, Phys. Rev. B 54 (1996) 9131.
[3] G. Song, A. Remhof, K. Theis-Bröhl, H. Zabel, Phys. Rev. Lett. 79 (1997) 5062.
[4] U. Laudahn, A. Pundt, M. Bicker, U.v. Hülsen, U. Geyer, T. Wagner, R. Kirchheim, J. Alloys Comp. 293 (1999) 490.
[5] A. Pundt, R. Kirchheim, Ann. Rev. Mater. Res. 36 (2006) 555.
[6] A. Pundt, M. Getzlaff, M. Bode, R. Kirchheim, R. Wiesendanger, Phys. Rev. B 61 (2000) 9964.
[7] A. Pundt, U. Laudahn, U.v. Hülsen, U. Geyer, T. Wagner, M. Getzlaff, M. Bode, R. Wiesendanger, R. Kirchheim, Mater. Res. Soc. Symp. Proc. 594 (2000) 75.
[8] K. Nörthemann, R. Kirchheim, A. Pundt, J. Alloys Comp. 356 (2003) 541.
[9] K. Nörthemann, A. Pundt, Phys. Rev. B 78 (2008) 014105.
[10] A. Pundt, Habilitation Thesis, Nanoskalige Metall-Wasserstoff-Systeme, University of Göttingen, <http://hdl.handle.net/11858/00-1735-0000-0006-B458-2>, 2005.
[11] S. Wagner, H.T. Uchida, V. Burlaka, M. Vlach, M. Vlcek, F. Lukac, J. Cizek, C. Baehtz, A. Bell, A. Pundt, Scripta Mater. 64 (2011) 978.
[12] U. Laudahn, Ph.D. Thesis, Spannungen und Dehnung von mit Wasserstoff beladenen Nb-Einfach- und Pd-Nb-Vielfachschichten, University of Göttingen, 1998.
[13] B. Heuser, M.M.C. Allain, W.C. Chen, Phys. Rev. B 66 (2002) 155419.
[14] M. Dornheim, Ph.D. Thesis, Spannungen, Dehnungnen und Lage der Phasengrenzenin dünnen Nb- und Y-Schichten bei Wasserstoffbe- und -entladung, University of Göttingen, <http://hdl.handle.net/11858/00-1735-0000-0006-B420-D>, 2002.
[15] H. Zabel, A. Weidinger, Commun. Condens. Mater. Phys. 17 (1995) 239.
[16] P.M. Reimer, H. Zabel, C.P. Flynn, J.A. Dura, K. Ritley, Z. Phys. Chem. 181 (1993) 375.
[17] K. Nörthemann, A. Pundt, Phys. Rev. B 83 (2011) 155420.
[18] R. Schwarz, A. Khachaturyan, Acta Mater. 54 (2006) 313.
[19] F.L. Larche, Ann. Rev. Mater. Sci. 20 (1990) 83.
[20] J.W. Cahn, F. Larche, Acta Metal. 32 (1984) 1915.
[21] F. Kroupa, Czech. J. Phys. B 10 (1960) 284.
[22] W.C. Johnson, P.W. Voorhees, J. Appl. Phys. 61 (1987) 1610.
[23] S. Wagner, M. Moser, C. Greubel, K. Peeper, P. Reichart, A. Pundt, G. Dollinger, Int. J. Hydrogen Energy 38 (2013) 13822.
[24] A. Kumar, M. Gautam, A. Subramaniam, J. Appl. Phys. 115 (2014) 193509.
[25] G. Reisfeld, N.M. Jisrawi, M.W. Ruckman, M. Strongin, Phys. Rev. B 53 (1996) 4974.
[26] G. Song, M. Geitz, A. Abromeit, H. Zabel, Phys. Rev. B 54 (1996) 14093.
[27] J. Bloch, B. Hjörvarsson, S. Olsson, R. Brukas, Phys. Rev. B 75 (2007) 165418.
[28] G.K. Palsson, A.R. Rennie, B. Hjörvarsson, Phys. Rev. B 78 (2008) 104118.
[29] C. Gente, M. Oehring, R. Bormann, Phys. Rev. B 48 (1993) 13244.
[30] R. Busch, F. Gärtner, C. Borchers, P. Haasen, R. Bormann, Acta Metall. Mater. 43 (1995) 3467.
[31] C. Michaelsen, Phil. Mag. 72 (1995) 813.